Inorg. Chem. **2004**, *43*, 923–930

Enzymatic Mechanism of Fe-Only Hydrogenase: Density Functional Study on H–H Making/Breaking at the Diiron Cluster with Concerted Proton and Electron Transfers

Taijin Zhou,* Yirong Mo,† Aimin Liu,‡ Zhaohui Zhou, and K. R. Tsai

Department of Chemistry and the State Key Laboratory for Physical Chemistry of the Solid Surface, Xiamen University, Xiamen 361005, People's Republic of China

Received March 3, 2003

The mechanism of the enzymatic hydrogen bond forming/breaking ($2H^+ + 2e \leftrightarrows H_2$) and the plausible charge and spin states of the catalytic diiron subcluster $[FeFe]_H$ of the H cluster in Fe-only hydrogenases are probed computationally by the density functional theory. It is found that the active center $[FeFe]_H$ can be rationally simulated as $\{[H](CH_3S)(CO)(CN^-)Fe_p(CO_b)(\mu\text{-SRS})Fe_d(CO)(CN^-)L\}$, where the monovalence [H] stands for the $[4Fe4S]_H^{2+}$ subcluster bridged to the $[FeFe]_H$ moiety, (CH_3S) represents a Cys–S, and (CO_b) represents a bridging CO. L could be a CO, H_2O, H^-, H_2, or a vacant coordination site on Fe_d. Model structures of possible redox states are optimized and compared with the X-ray crystallographic structures and FTIR experimental data. On the basis of the optimal structures, we study the most favorable path of concerted proton transfer and electron transfer in H_2-forming/breaking reactions at $[FeFe]_H$. Previous mechanisms derived from quantum chemical computations of Fe-only hydrogenases (Cao, Z.; Hall, M. B. *J. Am. Chem. Soc.* **2001**, *123*, 3734; Fan, H.; Hall, M. B. *J. Am. Chem. Soc.* **2001**, *123*, 3828) involved an unidentified bridging residue (μ-SRS), which is either a propanedithiolate or dithiomethylamine. Our proposed mechanism, however, does not require such a ligand but makes use of a shuttle of oxidation states of the iron atoms and a reaction site between the two iron atoms. Therefore, the hydride H_b^- (bridged to Fe_p and Fe_d) and η^2-H_2 at Fe_p or Fe_d most possibly play key roles in the dihydrogen reversible oxidation at the $[FeFe]_H$ active center. This suggested way of H_2 formation/splitting is reminiscent of the mechanism of [NiFe] hydrogenases and therefore would unify the mechanisms of the two related enzymes.

Introduction

Because hydrogen (H_2) is regarded as a potential future energy resource, the efficient generation, storage, and oxidative conversion of H_2 have been the subject of intense studies. Before mankind has been able to design and synthesize catalysts for fast and economical production of H_2 or efficient conversion of H_2 into protons and electrons, nature has evolved a family of enzymes called hydrogenases (or hereafter H_2ases), which are capable of catalyzing the reversible two-electron oxidation of H_2 as $H_2 \leftrightarrows 2H^+ + 2e^-$. H_2ases constitute the core of H_2 metabolism that is essential to many microorganisms of biotechnological interest.[1,2] The microorganisms can use H_2 as a source of electrons and protons or generate H_2 by reducing protons. In the organisms so far studied, H_2ases as metalloenzymes are mainly grouped into two classes:[3–6] [NiFe]H_2ases (which may include [NiFeSe]H_2ase), which most often catalyze the forward reaction in which H_2 is consumed,[7–14] and [FeFe]H_2ases

* Author to whom correspondence should be addressed. E-mail: tjzhou@xmu.edu.cn. Fax: +86-592-2183795.

† Permanent address: Department of Chemistry, Western Michigan University, Kalamazoo, MI 49008.

‡ Permanent address: Department of Biochemistry, University of Mississippi Medical Center, Jackson, MS 39216.

(1) Cammack, R. *Nature* **1999**, *397*, 214.
(2) Collman, J. P. *Nat. Struct. Biol.* **1996**, *3*, 213.
(3) Holm, R. H.; Kennepohl, P.; Solomon, E. I. *Chem. Rev.* **1996**, *96*, 2239.
(4) Thauer, R. K.; Klein, A. R.; Hartmann, G. C. *Chem. Rev.* **1996**, *96*, 3031.
(5) Albracht, S. P. J. *Biochim. Biophys. Acta* **1994**, *1118*, 167.
(6) Frey, M. *ChemBioChem* **2002**, *3*, 153.
(7) Volbeda, A.; Charon, M.-H.; Plras, C.; Hatchiklan, E. C.; Frey, M.; Fontecilla-Camps, J. C. *Nature* **1995**, *373*, 580.
(8) Volbeda, A.; Garcin, E.; Piras, C.; de Lacey, A. L.; Fernandez, V. M.; Hatchikian, E. C.; Frey, M.; Fontecilla-Camps, J. C. *J. Am. Chem. Soc.* **1996**, *118*, 12989.
(9) Frey, M. *Struct. Bonding* **1998**, *90*, 97.
(10) Lenz, O.; Friedrich, B. *Proc. Natl. Acad. Sci. U.S.A.* **1998**, *98*, 12474.
(11) Cammack, R., Reedijk, J., Ed. *Bioinorganic Catalysis*; Marcel Dekker: New York, 1993; pp 189−225.

10.1021/ic0342301 CCC: $27.50
Published on Web 01/06/2004

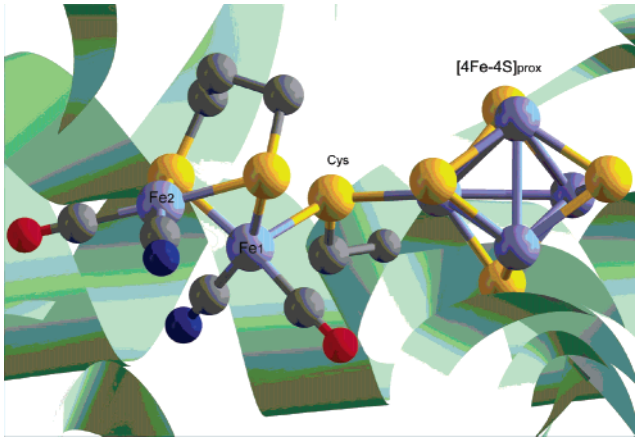

Figure 1. Three-dimensional structure of the H cluster in the DdH enzyme and its proximal protein environment revealed by the X-ray crystallographic study.[17]

(iron-only H_2ases), which catalyze the reduction of protons as terminal electron acceptors to yield H_2 and thus mainly function in H_2 production.[15−24] The [NiFe]H_2ase in the bacterium *Desulfovibrio gigas* (DvH) has been crystallized in the air-oxidized form and its structure solved by Volbeda et al.[7,8] The crystal structure of [NiFe]H_2ase reveals that the active center is composed of a [Ni] and a [Fe] bridged by two cysteinyl−S, as well as an oxygenic species, μ-O, which is assumed to be removed during the reductive activation of the enzyme.[25]

For [FeFe]H_2ases, recently two X-ray crystallographic structures of the enzymes from the bacteria *Clostridium pasterianum* (CpI)[15] and *Desulfovibrio desulfuricans* (DdH)[17] have been resolved. Compared with the [NiFe]H_2ase, the [FeFe]H_2ases are highly evolved catalysts. Under optimal conditions, each molecule of DdH can produce 9000 H_2/s^{-1} at 30 °C; for CpI, the figure is 6000 s^{-1}.[1,26] DdH contains three evenly spaced [4Fe−4S] clusters, which connect the active site with the molecular surface. The [6Fe−6S] cluster, termed H cluster (Figure 1), consists of a $[4Fe-4S]_H$ cuboidal cluster covalently bridged to an unusual $[FeFe]_H$ diiron cluster by a cysteinyl thiolate, S(Cys). The relative location of each of the metal clusters in the H_2ase crystal structures depicts probable electron-transfer (ET) pathways. Peters et al.[15,16] and Nicolet et al.[17−20] have proposed a similar pathway of the proton transfer (PT) and ET to the H cluster based on their respective protein structures. The pathway consists of a few conserved amino acid side chains along with protein-bound water molecules. A potential channel for the delivery of H_2 molecules, which is hydrophobic and connects the active site to the molecular surface, has also been proposed.[1,2,15−20]

The successive crystal structure determination of the above three H_2ases and the discovery that the DvH (and later, the CpI and DdH as well) contains cyanide in its prosthetic group, as well as the technological significance of H_2 as a potential resource of clean fuel, have greatly piqued the interest of chemical, biochemical, and biophysical scientists. The prosthetic groups of these H_2ases have been studied intensively with a wide variety of spectroscopic techniques such as EPR, ENDOR, Mössbauer, resonance Raman, and FTIR spectroscopy.[26−29] In particular, the FTIR spectra of the three redox states for DdH were investigated, and the results provided insights into the correlation between the geometrical structures and redox states in the H cluster. It is now generally believed that the $[4Fe-4S]_H$ always appears in the EPR-silent 2+ state, or $[4Fe-4S]_H^{2+}$, and the $[FeFe]_H$ of DdH or CpI in both oxidized and reduced states are EPR-silent and may be better symbolized as $[Fe^{II}Fe^{II}]_{H_{ox}}$ (H_{ox} in short) and $[Fe^{I}Fe^{I}]_{H_{red}}$ (or H_{red}), respectively. In contrast, the semireduced diiron cluster, symbolized as H_s, in DdH or CpI is EPR-active ($S = {}^1/_2$) and can be expressed as $[Fe^{II}Fe^{I}]_{H_s}$. These three states exhibit distinctive yet different IR bands for the CO ligands respectively (i.e., for CO in H_{ox}, 1847, 1983, and 2007 cm^{-1}; in H_{red}, 1894, 1916, 1940, and 1965 cm^{-1}; and in H_s, 1802, 1940, and 1965 cm^{-1}).[19,30] Pickett et al. pointed out that the fully reduced Fe^IFe^I species favors the terminal CO conformation and the Fe^IFe^{II} transient bridging CO intermediate can be generated by the one-electron oxidation of an Fe^IFe^I precursor bearing the thioether group. The observed IR spectra for CN and CO are consistent with the CO-inhibited paramagnetic center of [FeFe]H_2-ases.[31,32]

Both of the cationic iron atoms in $[FeFe]_H$, assumed to be the active center, adopt an octahedral coordination mode and are bridged to each other by three nonprotein atoms, namely, two μ-S and one putative CO_b. While $[4Fe-4S]_H$ and $[FeFe]_H$ are similarly associated by a cysteinyl−S in DdH, the two [Fe]'s of the $[FeFe]_H$ cluster are bridged by two μ-S, which

(12) Sellmann, D.; Geipel, F.; Moll, M. *Angew. Chem., Int. Ed.* **2000**, *39*, 561.
(13) Bertrand, P.; Dole, F.; Asso, M.; Guigliarelli, B. *J. Biol. Inorg. Chem.* **2002**, *5*, 682.
(14) Fong, T. P.; Forde, C. E.; Lough, A. J.; Morris, R. H.; Rigo, P.; Rocchini, E.; Stephan, T. *J. Chem. Soc., Dalton Trans.* **1999**, 4475.
(15) Peters, J. W.; Lanzilotta, W. N.; Lemon, B. J.; Seefeldt, L. C. *Science* **1998**, *282*, 1853 (Errata: **2002**, *283*, 35).
(16) Peters, J. W. *Curr. Opin. Struct. Biol.* **1999**, *6*, 670.
(17) Nicolet, Y.; Piras, C.; Legrand, P.; Hatchikian, E. C.; Fontecilla-Camps, J. C. *Struct. Fold Des.* **1999**, *7*, 13.
(18) Nicolet, Y.; Lemon, B. J.; Fontecilla-Camps, J. C.; Peters, J. W. *TIBS* **2000**, *25*, 138.
(19) Nicolet, Y.; Lacey, A. L.; Vernede, X. M.; Fernandez, V. M.; Hatchikian, E. C.; Fontecilla-Camps, J. C. *J. Am. Chem. Soc.* **2001**, *123*, 1596.
(20) Pierik, A. J.; Hagen, W. R.; Redeker, J. S.; Wolbert, R. B. G.; Boersma, M.; Verhagen, M. F. J. M.; Grande, H. J.; Veeger, C.; Mutsaers, P. H. A.; Sand, R. H.; Dunham, W. R. *Eur. J. Biochem.* **1992**, *209*, 63.
(21) Niu, S.; Thomson, L. M.; Hall, M. B. *J. Am. Chem. Soc.* **1999**, *121*, 4000.
(22) Cao, Z.; Hall, M. B. *J. Am. Chem. Soc.* **2001**, *123*, 3734.
(23) Fan, H.; Hall, M. B. *J. Am. Chem. Soc.* **2001**, *123*, 3828.
(24) Nicolet, Y.; Cavazza, C.; Fontecilla-Camps, J. C. *J. Inorg. Biochem.* **2002**, *91*, 1.
(25) Pavlov, M.; Siegbahn, P. E. M.; Blomberg, M. R. A.; Crabtree, R. H. *J. Am. Chem. Soc.* **1998**, *120*, 548.
(26) Adams, M. W. W. *Biochim. Biophys. Acta* **1990**, *1020*, 115.
(27) Adams, M. W. W.; Stiefel, E. I. *Curr. Opin. Chem. Biol.* **2000**, *4*, 214.
(28) Popescu, C. V.; Munck, E. *J. Am. Chem. Soc.* **1999**, *121*, 7877.
(29) Pereira, A. S.; Tavares, P.; Moura, I.; Moura, J. G.; Huynh, B. H. *J. Am. Chem. Soc.* **2001**, *123*, 2771.
(30) Liu, Z. P.; Hu, P. *J. Am. Chem. Soc.* **2002**, *124*, 5175.
(31) (a) Razavet, M.; Borg, S. J.; George, S. J.; Best, S. P.; Fairhurst, S. A.; Pickett, C. J. *Chem. Commun.* **2002**, 700. (b) George, S. J.; Cui, Z.; Razavet, M.; Pickett, C. J. *Chem.−−Eur. J.* **2002**, *8*, 4037.
(32) Yang, X.; Razavet, M.; Wang, X. B.; Pickett, C. J.; Wang, L. S. *J. Phys. Chem. A* **2003**, *107*, 4612.

are linked together and initially modeled as μ-propanedithiolate (PDT) and by an unspecified μ-O.[17] Recently, on the basis of crystallographic and FTIR spectroscopic evidence from DdH, Nicolet et al. claimed that the previously observed CO_b ligand in CpI (probably in the oxidized state) is terminally bound (CO_t) in the reduced DdH,[18] and the transition of the CO_b to CO_t affects mostly the C atom, whereas the O atom essentially keeps the same position with respect to the two iron ions.[19] Furthermore, it has also been proposed that, from stereochemical and mechanistic considerations, the original assignment of the μ-SRS to PDT (i.e., R = $(CH_2)_3$) might be incorrect. A dithiomethylamine (DTMA; i.e., R = CH_2NHCH_2) assignment, although still speculative, seems to make more sense because the latter would contribute a more basic, NH bridgehead that might be more effective for the heterolytic splitting of H−H. In addition, the distance between the NH of DTMA and a Cys178[19] residue can better rationalize the observed internuclear distance of 3.2 Å than that between the central CH_2 of μ-PDT and Cys178.

The $[FeFe]_H$ is well modeled by easily prepared and classical organometallic complexes, $(\mu\text{-SRS})[Fe(CO)_2L]_2$ with L = CO, CN^-, PMe_3, etc., and R = $-(CH_2)_3-$, or $-(CH_2NMeCH_2)-$.[31−53] Important information about the charge, spin, and chemical states as well as the ligand exchange reactivity of $[FeFe]_H$ has been derived from the synthesis and characterization of $(\mu\text{-SRS})[Fe(CO)_2L]_2$. It should be noted that known structures show the Fe−Fe internuclear distance of around 2.5 Å,[33,36,37] well within the bonding range and in accordance with the 18-electron rule.[38] Particularly, the synthetic dinuclear iron models reported independently by Gloaguen et al.,[41,44] Zhao et al., [42] and Nehring et al. [43] present significant H_2 molecule formation via reduction/protonation and H_2/D_2 exchange activity.

Despite numerous discussions on the possible mechanisms for H_2ase,[1,2,9,15−20,26,27,54] further quantitative analyses are pivotal for the future engineering of H_2ases with higher activity as well as the design of biomimetic materials to simulate the functions of H_2ases. In particular, computational studies on the structures and electronic states of the H cluster, transition state, and energy barrier, as well as vibrational frequencies of characteristic ligands, are indispensable to gain insights into the mechanism of enzymatic H−H bond making/breaking. Among various feasible methodologies, the hybrid density functional theory (DFT), which takes the electron correlation into account but retains the computational efficiency, has shown its reliability and popularity in modeling metalloenzymes.[55,56] Up to now, several groups[21−23,25,30,39,50,57−63] have attempted to model the [NiFe]-H_2ase and $[FeFe]H_2$ases with the hydrid DFT method. On the basis of the DFT optimal structures for $[FeFe]_H$, the high correlation between the computed IR frequencies of the CO_b, CO, and CN ligands, and the known IR frequencies of these ligands in the $[FeFe]_H$ of DdH,[22,30] strong theoretical supports have been garnered for a low-charge and low-spin diiron active center as previously inferred from EPR, ENDO, and Mössbauer spectroscopy.[26−29] A mechanism for the η^2-H_2 activation by side-on coordination at a vacant site of the Fe^I-Fe^{II} active center and the heterolytic splitting of the H−H bond assisted by an adjacent PDT−thiolate−μ-S was proposed by Cao and Hall.[22] The mechanism was later refined by replacing the PDT with a DTMA based on further theoretical analyses.[23,30] Bruschi et al. pointed out that H_2 can bind to Fe_p and its activation, involving both iron atoms and one of the bridging sulfur ligands, is associated with a very low activation energy, leading to intermediate species characterized by a μ-H atom.[63]

In view of the recent progresses in experimental and theoretical studies on the enzymatic mechanism of [FeFe]-H_2ases and the fact that all of the DFT studies on H_2ases catalysis so far have been focused on the H−H bond breaking, it is desirable to explore the enzymatic mechanism

(33) Erica, J. L.; Georgakaki, I. P.; Reibenspies, J. H.; Darensbourg, M. Y. *Angew. Chem., Int. Ed.* **1999**, *38*, 3178.
(34) Alban, L. C.; Stephen, P. B.; Stacey, B.; Sian, C. D.; David, J. E.; David, L. H.; Christopher, J. P. *Chem. Commun.* **1999**, 2285.
(35) Kaasjager, V. E.; Henderson, R. K.; Bouwman, E.; Lutz, M.; Spek, A. L.; Reedijk, J. *Angew. Chem., Int. Ed.* **1998**, *37*, 1668.
(36) Liaw, W. F.; Lee, N. H.; Chen, C. H.; Lee, C. M.; Lee, G. H.; Peng, S. M. *J. Am. Chem. Soc.* **2000**, *122*, 488.
(37) Schmidt, M.; Contakes, S. M.; Rauchfuss, T. B. *J. Am. Chem. Soc.* **1999**, *121*, 9736.
(38) Darensbourg, M. Y.; Lyon, E. J.; Smee, J. J. *Coord. Chem. Rev.* **2000**, *206*, 533.
(39) Lawrence, J. D.; Li, H.; Rauchfuss, T. B. *Chem. Commun.* **2001**, 1482.
(40) Lyon, E. J.; Georgakaki, I. P.; Reibenspies, J. H.; Darensbourg, M. Y. *J. Am. Chem. Soc.* **2001**, *123*, 3268.
(41) Gloaguen, F.; Lawrence, J. D.; Rauchfuss, T. B. *J. Am. Chem. Soc.* **2001**, *123*, 9476.
(42) (a) Zhao, X.; Georgakaki, I. P.; Miller, M. L.; Yarbrough, J. C.; Darcensbourg, M. Y. *J. Am. Chem. Soc.* **2001**, *123*, 9710. (b) Zhao, X.; Georgakaki, I. P.; Miller, M. L.; Mejia-Rodriguez, R.; Chiang, C. Y.; Darcensbourg, M. Y. *Inorg. Chem.* **2002**, *41*, 3917. (c) Zhao, X.; Chiang, C. Y.; Miller, M. L.; Rampersad, M. V.; Darcensbourg, M. Y. *J. Am. Chem. Soc.* **2003**, *125*, 518.
(43) Nehring, J. L.; Heinekey, D. M. *Inorg. Chem.* **2003**, *42*, 4288.
(44) Gloaguen, F.; Lawrence, J. D.; Rauchfuss, T. B.; Benard, M.; Rohmer, M.-M. *Inorg. Chem.* **2002**, *41*, 6573.
(45) Arabi, X. S.; Matheu, R.; Poilblanc, R. J. *J. Organomet. Chem.* **1979**, *177*, 199.
(46) Lawrence, J. D.; Li, H.; Rauchfuss, T. B.; Benard, M.; Rohmer, M.-M. *Angew. Chem., Int. Ed.* **2001**, *40*, 1768.
(47) Li, H.; Rauchfuss, T. B. *J. Am. Chem. Soc.* **2001**, *124*, 726.
(48) Curtis, C. J.; Miedaner, A.; Ciancanelli, R.; Ellis, W. W.; Noll, B. C.; DuBois, M. R.; DuBois, D. L. *Inorg. Chem.* **2003**, *42*, 216.
(49) Gloaguen, F.; Lawrence, J. D.; Schmidt, M.; Wilson, S. R.; Thomas, B.; Rauchfuss, T. B. *J. Am. Chem. Soc.* **2001**, *123*, 12518.
(50) Georgakaki, I. P.; Thomson, L. M.; Lyon, E. J.; Hall, M. B.; Darensbourg, M. Y. *Coord. Chem. Rev.* **2003**, *238*, 255.
(51) Lawrence, J. D.; Rauchfuss, T. B.; Wilson, S. R. *Inorg. Chem.* **2002**, *41*, 6193.
(52) Lawrence, J. D.; Rauchfuss, T. B.; Wilson, S. R. *Inorg. Chem.* **2002**, *41*, 6193.
(53) Darensbourg, M. Y.; Lyon, E. J.; Zhao, X.; Georgakaki, I. P. *Proc. Natl. Acad. Sci. U.S.A.* **2003**, *100*, 3683.
(54) Dole, F.; Fournel, A.; Magro, V.; Hatchikian, E. C.; Bertrand, P.; Guigliarelli, B. *Biochemistry* **1997**, *36*, 7847.
(55) Niu, S. Q.; Hall, M. B. *Chem. Rev.* **2000**, *100*, 353.
(56) Frenking, G.; Frohlich, N. *Chem. Rev.* **2000**, *100*, 717.
(57) Pavlov, M.; Blomberg, M. R. A.; Siegbahn, P. E. M. *Int. J. Quantum Chem.* **1999**, *73*, 197.
(58) Li, S.; Hall, M. B. *Inorg. Chem.* **2001**, *40*, 18.
(59) Siegbahn, P. E. M.; Eriksson, L.; Himo, F.; Pavlov, M. *J. Phys. Chem. B* **1998**, *102*, 10622.
(60) Siegbahn, P. E. M.; Margareta, R. A.; Blomberg, M. R. A.; Crabtree, P. R. H. *J. Biol. Inorg. Chem.* **2001**, *6*, 460.
(61) De Gioia, L.; Fantucci, P.; Guigliarelli, B.; Bertrand, P. *Int. J. Quantum Chem.* **1999**, *73*, 187.
(62) De Gioia, L.; Fantucci, P.; Guigliarelli, B.; Bertrand, P. *Inorg. Chem.* **1999**, *38*, 2658.
(63) (a) Bruschi, M.; Fantucci, P.; Gioia, L. *Inorg. Chem.* **2002**, *41*, 1421. (b) Bruschi, M.; Fantucci, P.; Gioia, L. *Inorg. Chem.* **2003**, *42*, 4773.

of the H−H bond making in [FeFe]H_2ases with computational tools. Our major interest lies in the evolution of the spin/charge state of the diiron $[FeFe]_H$ cluster as well as the rational pathways of PT and ET in the process of H_2 production.

Computational Details

Throughout the paper, all of the calculations were performed using the DFT program DMol[3] from Cerius[2] and Materials Studio software package.[64] DMol[3] utilizes a basis set of numeric atomic functions, which are in general more complete than a comparable set of linearly independent Gaussian functions, as most often adopted, and have been demonstrated to have negligible basis-set superposition errors.[64b]

The geometries of various models have been optimized by local DFT methods, specifically with the Perdew−Wang (1992) functional. The local spin-density approximation can be used to accurately predict structures, vibrations, and relative energies of covalent systems. Stationary points on a hypersurface have been located by means of energy-gradient techniques. In Dmol[3], the second derivatives are numerically computed by finite differences of the first derivatives. A full vibrational analysis has been performed to further characterize each stationary point. The Dmol[3] uses fast convergent three-dimensional numerical integrations to calculate matrix elements occurring in the Ritz variation method. As for the basis sets, we adopt the double numerical with d functions (DND) for all of the atoms. The size of the DND basis set is comparable to the standard Gaussian 6-31G* basis set. However, the numerical basis sets, which are exact solutions to the Kohn−Sham equations for the atoms,[64b] are much more accurate than a Gaussian basis set of the same size. The search for a transition structure (TS) comprises repeated steps of computations with the linear synchronous transit (LST)[65] and quadratic synchronous transit (QST)[66] methods. The LST procedure roughly locates a maximum along a path connecting two structures and provides a guess for the TS connecting them. A subsequent cycle of QST refinements involving a Brent line searches along the QST line, followed by an energy minimization of the maximum structure perpendicular to the QST line, and finally determines the TS.

Results and Discussion

Chemical Models of $[FeFe]_H$ for CpI and DdH. The H cluster in the H_2ases has been experimentally studied in three different forms (see Figure 1 in ref 40): (1) the partially oxidized form, where one of the irons, putatively $[Fe_d]$, is weakly bound by a water molecule; (2) the reduced form, where the H_2O is released from Fe_d and replaced by a H (or H_2) or a vacant coordination site on Fe_d, which is generally considered to be the primary catalytic center;[15−20] (3) the deactivated form, where a CO displaces the terminally bound H_2O around Fe_d. In the current paper, we intend to computationally explore the states of the H-cluster during the reaction process with cluster models, with the environmental effect inexplicitly taken into account. The models were built up based on the X-ray crystallographically determined structural coordinates of CpI and DdH[15,17,19] and by taking in the knowledge from the synthetic model complexes. In the crystal structures, the $[FeFe]_H$ consists of two octahedrally liganded Fe atoms that bind μ-SRS and a total of two CN^- and three CO ligands, of which one may be CO_b. The terminal N of each CN^- may form a H bond with the adjacent amino acid residues, and the CO ligands occupy hydrophobic pockets. However, the dicyano dianion in the synthetic model complexes is stabilized by quaternary ammonium cations as counterions.[38,40] Thus, in [FeFe]H_2ases, a dicyano anionic $[FeFe]_H$ may have charge compensation by H bonding to adjacent cationic residues. In other words, the chemical model can be envisaged as an anion. Darensbourg et al.[38,40] have pointed out that the CO ligands in $[FeFe]_H$ can be exchanged and stabilized by $CN^-\cdots H^+$ (here the dotted line denotes a H bond). Consequently, there would be one CN^- to each [Fe] in $[FeFe]_H$,[18] and the model $\{^-(NC)(CO)([H]SCH_3)Fe_p[(CO_b)(\mu\text{-SRS})]Fe_d(CO)(CN)^-L\}$ can serve as an initial chemical model for the catalytic center $[FeFe]_H$ in iron-only H_2ases. In the above model, L can be a ligand such as CO, H_2O, H^-, H_2, or simply a vacant coordination site on Fe_d. The μ-SRS in DdH was assigned initially as PDT[17] and later as DTMA by Nicolet et al.[19] It has been found that $[Ni(Et_2PCH_2NMeCH_2PEt_2)_2]^{2+}$ or $[Ni(PNP)_2]^{2+}$ catalyzes the electrochemical oxidation of H_2 and reacts with H_2 to form complexes in which the hydride ligand is associated with nickel and the proton is bound by nitrogen. Rapid exchange occurs between these two sites.[48] However, although the diiron azadithiolates $Fe_2[(SCH_2)_2NR](CO)_6$ and dicyanide complex $(NEt_4)_2[Fe_2\{(SCH_2)_2NMe\}(CO)_4(CN)_2]$ have been prepared,[46,47] evidence is elusive for the participation of the nitrogen atom of $(SCH_2)_2NR$ in the H_2-forming/breaking reaction. Importantly, it is experimentally verified that the hydride [$Fe^{II}-H-Fe^{II}$] can be produced via the protonation of the Fe^IFe^I model complexes such as $Fe_2(S_2C_3H_6)(CO)_4(PMe_3)_2$ (here we denote this complex as **M1**; thus, the protonation process is $\mathbf{M1} + H^+ \rightarrow \mathbf{M1}H^+$), and subsequently H_2 is produced by the reaction $\mathbf{M1}H^+ + H^+ + 2e \rightarrow \mathbf{M1} + H_2$.[41−44] Therefore, in this paper, we start from model $[FeFe]_{H_{red}} = \mathbf{1}[-2,0]$ (as shown in Figure 2) determined experimentally, where PDT is recommended.[17] To make the description concise throughout the paper, we use label $\boldsymbol{x}[x_1,x_2]$ to represent a model, where $\boldsymbol{x}$ refers to a serial number and x_1 and x_2 are the charge and spin states of the model, respectively.

Mechanism of H_2 Generation in $[FeFe]_H$. We investigate the reaction process of $2H^+ + 2e + [FeFe]_{H_{red}} \rightarrow \cdots \rightarrow [FeFe]_{H_{red}} + H_2$ starting with the model $\mathbf{1}[-2,0]$ as shown in Figure 2. Obviously, as a catalyst, $[FeFe]_H$ should be invariant in the cycle of H_2 generation. We want to address the following issues: (i) What is the most likely structure of $[FeFe]_H$? (ii) What are the intermediates and reaction steps in the catalytic cycle? (iii) What insights can be garnered

(64) (a) Delley, B. *J. Chem. Phys.* **1990**, *92*, 508. (b) Delley, B. In *Density Functional Theory: A Tool for Chemistry*; Seminario, J. M., Politzer, P., Eds.; Elsevier: Amsterdam, The Netherlands, 1995.
(65) Halgren, T. A.; Lipscomb, W. N. *Chem. Phys. Lett.* **1977**, *49*, 225.
(66) Frisch, M. J.; Trucks, G. W.; Schlegel, H. B.; Gill, P. M. W.; Johnson, B. G.; Robb, M. A.; Cheeseman, J. R.; Keith, T.; Petersson, G. A.; Montgomery, J. A.; Raghavachari, K.; Al-Laham, M. A.; Zakrzewski, V. G.; Ortiz, J. V.; Foresman, J. B.; Peng, C. Y.; Ayala, P. Y.; Chen, W.; Wong, M. W.; Andres, J. L.; Replogle, E. S.; Gomperts, R.; Martin, R. L.; Fox, D. J.; Binkley, J. S.; Defrees, D. J.; Baker, J.; Stewart, J. P.; Head-Gordon, M.; Gonzalez, C.; Pople, J. A. *Gaussian 98*, A.3 ed.; Gaussian, Inc.: Pittsburgh, PA, 1999.

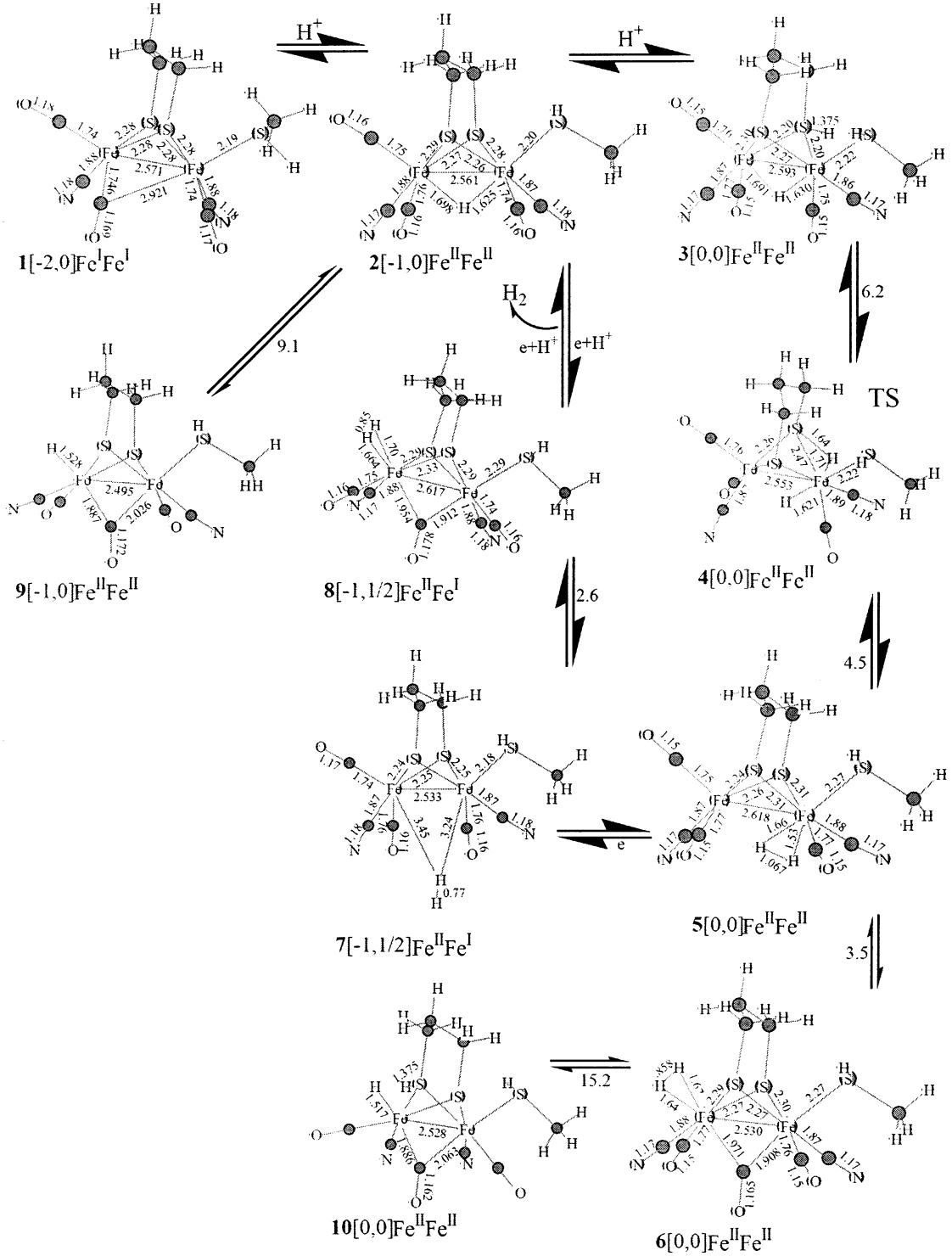

Figure 2. Optimal geometries of various probable models (**1**−**10**) in the process of $2H^+ + 2e \leftrightarrows H_2$ at $[FeFe]_{H_{res}}$. The values on the arrowheads are the energies (kcal/mol) at a temperature of 298 K. Highlighted arrowheads represent the preferable paths.

from the electronic structures of these redox states? First, excellent linear correlation between the computed and the observed CO frequencies for models **1**−**8** is found and shown in Figure 3.[22,23] This linear relationship is thus employed to predict the CO frequencies from calculated data. In fact, if we request the linear relationship to cross the origin, it would suggest a scaling factor of 0.9639 for the computed frequencies at the correlation factor $R^2 = 0.9863$. The predicted frequencies are further compared with the observed bands from the experiment in Tables 1 and 2.[19] Table 1 listed the major structural parameters and stretching frequencies of CO_b on **1**[−2,0]. The agreement between our data and others, particularly the experimental findings, legitimates **1**[−2,0] as a model for $[FeFe]_{H_{red}}$. In Figure 2, the bond distances of Fe−CO and Fe−CN^- are about 1.74−1.77 and 1.86−1.88 Å, respectively. The discrepancy between the ligands CO and CN^- lies in the fact that CO is a better π-electron acceptor than CN^-.[38] Thus, the CO bond lengths in the

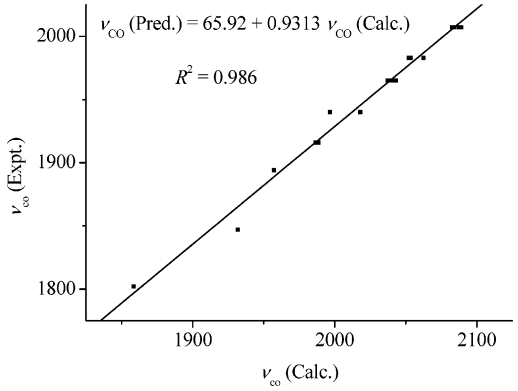

Figure 3. Linear fitting of the calculated CO stretching frequencies against the predicted data. The calculated CO stretching frequencies are taken from calculation results in models **1**−**3** and **5**−**8**.

Table 1. Comparison of Experimental Data and DFT-Optimized Results in the CO_b Part of $[FeFe]_{H_{red}}$

	model		
	a[a]	b[b]	**1**[−2,0]
CO_b-Fe_p bond length (Å)	2.40 (2.56)		2.921
CO_b-Fe_d bond length (Å)	1.69 (1.69)	1.794	1.746
Fe_p-Fe_d bond length (Å)	2.55 (2.61)	2.655	2.571
C−O bond length (Å)		1.185	1.169
$\nu(CO_b)$ (cm^{-1})	1894	1878	1889[c]

[a] Experimental data are obtained from ref 19. [b] DFT calculation data are from model **26**[−3,0] in ref 22. [c] The predicted CO stretching frequency is calculated according to the linear-fitting formula in Figure 3.

models are a measurement of the π-donor ability or the redox state of the iron ion. For instance, the CO bond is longer in the Fe^IFe^I (**1**) and $Fe^{II}Fe^I$ (**7** and **8**) models than in the Fe^{II}-Fe^{II} models (**3**−**6**) and is longer in negative charge models **1**, **2**, **7**, and **8** than in neutral models **3**−**6**. Simultaneously, the CO bond lengths (in Figure 2) are closely correlated with the CO frequencies (in Table 2). In models **6** and **8**, the bond lengths of CO_b are longer than those of CO_t; consequently, the CO_b frequencies are lower than those of CO_t. Similar conclusions can be drawn by the comparison of models **3**, **5**, and **6** with models **2** and **8**.

Next, we attempt to build a flowchart for the formation of H_2 in $[FeFe]H_2$ases and investigate the evolution of the structures of **1**[−2,0] combined with protons and electrons at various stages (Figure 2). Through the reaction of **1**[−2,0] + H^+ → **2**[−1,0], the incoming proton takes the middle position between two irons, Fe_p and Fe_d, and meanwhile, CO_b is shifted to the Fe_d side as a terminal CO_t ligand. This process can be written as $H^+ + [Fe^IFe^I](CO_b) \rightarrow [Fe^{II}Fe^{II}]H_b^-$ + CO_t. Optimization results indicate that **2**[−1,0] is energetically the most favorable state for the complex of system **1**[−2,0] and H^+. In **2**[−1,0], the bridging species is H_b, while the original CO_b turns out to be a terminal CO_t. Population analysis demonstrated that the H_b^- in **2**[−1,0] essentially is H_b^{δ} (Mulliken atomic charges $\delta = 0.143$e), and the bridging H is more like a hydrogen atom than an anion H^-. Thus, the electronic configuration of [FeFe] in **2** might be seen as a mixture of the three configurations CO_b-H_{ox}, CO_b-H_s, and CO_b-H_{red}. As a consequence, the CO_t stretching frequencies (1916, 1926, and 1963 cm^{-1}) in **2** can be seen as a mixture of 1916 cm^{-1} (H_s) and 1940 and 1965 cm^{-1} (H_s and H_{red}) (see Table 2). There is another possible complex of **1**[−2,0]

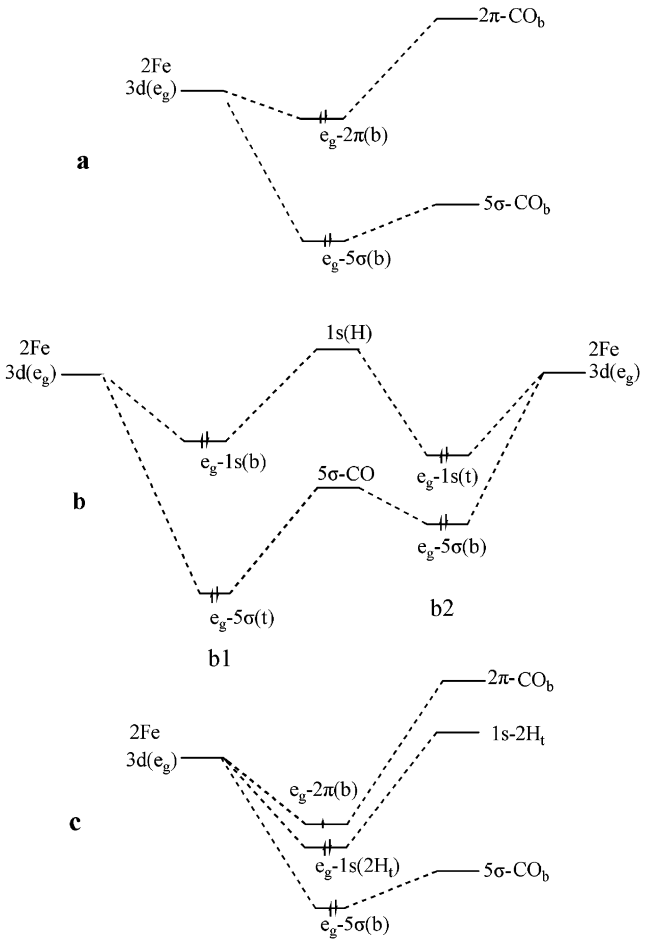

Figure 4. Simplified molecular-orbital diagram showing the interaction among CO_b, CO_t, H_b^-, H_t^-, and Fe(3d−e_g) (a) for model **1**[−2,0]; (b1) model **2**[−1,0]; (b2) model **9**[−1,0]; and (c) model **8**[$-1,^1/_2$].

Table 2. Comparison of the Calculated, Predicted, and Observed CO Frequencies (cm^{-1})[a]

species	calculated	predicted[b]	observed
1[−2,0]Fe^IFe^I	*1957.2*	*1889*	*1894*(b)
2[0,0]$Fe^{II}Fe^{II}$	1986.7, 1996.7, 2037.2	1916, 1926, 1963	1916(b), 1940(c,b), 1965(c,b)
3[0,0]$Fe^{II}Fe^{II}$	2043.0, 2052.2, 2082.5	1969, 1977, 2005	1965(c,b), 1983(a), 2007(a)
5[0,0]$Fe^{II}Fe^{II}$	2041.9, 2053.2, 2083.9	1968, 1978, 2007	1965(c,b), 1983(a), 2007(a)
6[0,0]$Fe^{II}Fe^{II}$	*1931.8*, 2062.5, 2087.2	*1865*, 1987, 2010	*1847*(a), 1983(a), 2007(a)
7[−1,1/2]$Fe^{II}Fe^I$	2039.4, 2053.6, 2089.1	1965, 1979, 2012	1965(b,c), 1983(a), 2007(a)
8[−1,1/2]$Fe^{II}Fe^I$	*1858.5*, 1988.7, 2018.0	*1797*, 1912, 1945	*1802*(c), 1916(b), 1940(b,c)

[a] The observed data are taken from ref 19. The symbol in parentheses denotes the redox state of the species: (a) as isolated, H_{ox}, (b) after reduction, H_{red}, and (c) after reoxidation, H_s. The italicized data correspond to the CO_b frequencies, and the others represent the CO_t frequencies. [b] The predicted ν_{CO} data are calculated according to the linear-fitting formula in Figure 3.

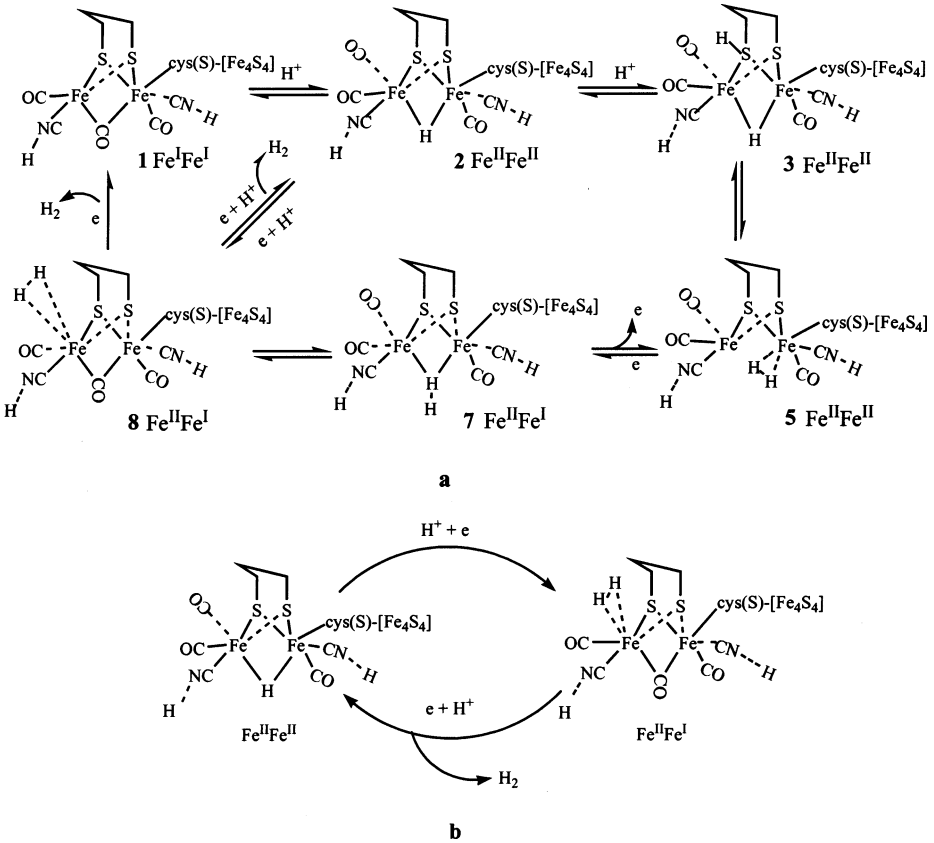

Figure 5. (a) Catalytic cycle on $[FeFe]_H$ and (b) simplified key steps in the catalytic cycle.

plus H^+ where CO_b is unchanged, but the incoming H^+ takes a terminal position (model **9**[−1,0]). However, the latter structure **9**[−1,0] is unstable by 9.1 kcal/mol compared with **2**[−1,0]. The reaction **2**[−1,0] → **9**[−1,0] occurs via ETs from $e_g-5\sigma(CO_t)$ and $e_g-1s(H_b)$ to $e_g-5\sigma(CO_b)$ and $e_g-1s(H_t)$ and is energetically unfavorable because the energy gap between $e_g-1s(H_t)$ and $e_g-1s(H_b)$ is smaller than that between $e_g-5\sigma(CO_t)$ and $e_g-5\sigma(CO_b)$ as shown in Figure 4b. As a matter of fact, these two cases are parallel to the structures **3**[0,0] and **10**[0,0] where the former is 13.4 kcal/mol more stable than the latter, as demonstrated in Figure 2. This implies that H_t^- is less stable than H_b^-. Is there any possibility that model **2**[−1,0] accepts an electron following the process **1**[−2,0] + H^+ → **2**[−1,0]? The answer might be no. This is due to the fact that all of the low-lying 3d bonding orbitals in Fe_p and Fe_d are almost fully occupied in **2**[−1,0], and the energy level of LUMO is so high that the probability of the reaction of **2**[−1,0] with another electron is very small. Therefore, **2**[−1,0] is nucleophilic, and its protonation most possibly results in **3**[0,0]. Interestingly, although μ-S is tetracoordinated in **3**[0,0], the (μ-S)−Fe bond remains strong; the bond lengths are basically unchanged. Because the negative charge of $H_b^{\delta-}$ is very small in **2**[−1,0] or **3**[0,0], $H_b^{\delta-}$ has a much smaller ion radius than the anion H^-. As a consequence, the relatively long distance of Fe−H (1.6 Å) implies that the $Fe_p\cdots H_b^{\delta-}\cdots Fe_d$ is a weak bond.[67] We further infer that the weakly bound $H^{\delta-}$ could attract the proton hanging on μ-S. This results in the formation of η^2-H_2 at Fe_p or model **5**[0,0]. The transformation from **3**[0,0] to **5**[0,0] needs to pass the transition state **4**[0,0]. The location of **4**[0,0] shows that the dihydrogen formation or breakage on Fe_p requires an activation energy of only 6.2−4.5 kcal/mol. Although the transformation from **5**[0,0] to **6**[0,0] is energetically favorable, it might be dynamically difficult because of the possible existence of nonclassical bonds $Fe_p-(\eta^2-H_2)$ (model **5**[0,0]) and $Fe_d-(\eta^2-H_2)$ (model **6**[0,0]), which are fairly stable in $[Fe^{II}Fe^{II}]$. The $Fe-(\eta^2-H_2)$ falls in the category of two-electrons-three-center (2e−3c) bonds.[68] Similar 2e−3c bonds have been found in CH_5^+,[69,70] methane dehydrogenation in the absence of O_2,[71] and the H−H activation by $[NiFe]H_2$ases.[21,25,39,57,60] When an electron enters **5**[0,0] or **6**[0,0], model **7**[−1,$^1/_2$] or **8**[−1,$^1/_2$] (active oxidized state $[FeFe]_{H_s}$) is generated. The comparison between Fe−(η^2-H_2) in **5**[0,0] and **7**[−1,$^1/_2$] (or **6**[0,0] and **8**[−1,$^1/_2$]) shows that the H−H distance in **7** (or **8**) becomes shorter than that in **5** (or **6**), while the distance between η^2-H_2 and Fe_p (or Fe_d) lengthens. This suggests that $Fe_p-(\eta^2-H_2)$ and $Fe_d-(\eta^2-H_2)$ are more active in $[Fe^{II}Fe^{I}]$ than in $[Fe^{II}Fe^{II}]$, and ET is the driving force for the H−H bond making/breaking at the Fe_p (or Fe_d) active center. Therefore, the evolution from **7**[−1,$^1/_2$] to **8**[−1,$^1/_2$] is easier than that from **5**[0,0] to **6**[0,0]. Because the structural data and predicted CO stretching frequencies listed in Figure 2 and Table 2 for models **2**−**8** are in good agreement with the experimental

(67) Bau, R.; Teller, R. G.; Kirtley, S. W.; Koetzle, T. F. *Acc. Chem. Res.* **1979**, *12*, 176.
(68) Kubas, G. J. *Acc. Chem. Res.* **1988**, *21*, 120.
(69) Scuseria, G. E. *Nature* **1993**, *366*, 512.
(70) Marx, D.; Parrinello, M. *Nature* **1995**, *375*, 216.
(71) Zhou, T.; Liu, A.; Mo, Y.; Zhang, H. *J. Phys. Chem. A* **2000**, *104*, 4505.

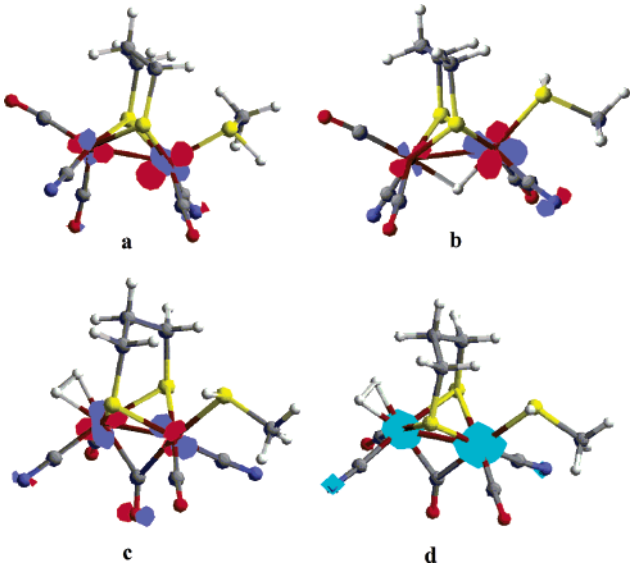

Figure 6. Frontier molecular orbitals and the spin-density map: (a) HOMO of **1**; (b) HOMO of **2**; (c) HOMO of **6**; (d) total spin density of **8**.

findings, we propose that **2**[−1,0], **7**[−1,$^1/_2$], and **8**[−1,$^1/_2$] would be the key structures in the catalytic cycle, whereas **3**[0,0], **5**[0,0], and **6**[0,0] are possible intermediates of comparable stabilities. On the basis of our calculations and the above discussion, the mechanism of reversible H_2 oxidation is summarized in Figure 5. In particular, Figure 5b shows that an electron and a proton would simultaneously arrive at $[FeFe]_H$ to avoid costly charge separation.

Compared with the mechanism proposed by Hall and coworkers,[22,23] our scheme highlights the importance of the hydride ($Fe-H_b-Fe$) in the reversible H_2 oxidation similar to the case of $[NiFe]H_2$ase.[21] It is rational to compare the function of the cationic [Ni] in $[NiFe]H_2$ases with the $[Fe_p]$ in $[FeFe]H_2$ases. The processes of dihydrogen production and dihydrogen uptake should be microscopically reversible. The existence of the hydride in $[FeFe]_H$ has been speculated.[19] Our mechanism also shows that a CO could rapidly alter from a bridging to an Fe_d terminal position, as pointed out by Nicolet et al.[18,19] and Bruschi et al.[63] Cao and Hall suggested that the first step of the H−H bond breaking only removes a single proton to the neighboring base center μ-S.[22] However, our computations reveal that the transformation from **6**[0,0] to **10**[0,0] is endothermic by 15.2 kcal/mol and thus does not seems energetically favorable, because the activation barrier must be higher than 15.2 kcal/mol.

In $[FeFe]_H$, both of the iron ions tend to satisfy the 18-electron rule. Thus, an Fe−Fe metal bond is formed if there is a surplus valence electron on each Fe ion in the valence state of Fe^IFe^I (model **1**). The short Fe−Fe distance indicates a strong metal−metal interaction. Liu and Hu[30] pointed out that the interaction of $e_g(2Fe)-5\sigma(CO_b)$ and $e_g(Fe_d)-2\pi(CO_b)$ plays key roles in the stabilization of $[Fe^IFe^I]CO_b-H_{red}$ (see Figure 4a). The full occupation of $e_g(Fe_d)-2\pi(CO_b)$ mainly strengthens the bonding between CO_b and Fe_d and leads to CO_b shifting toward Fe_d in **1**[−2,0]. The HOMO of model **1** is characterized by a large lobe underneath the $Fe-CO_b-Fe$ frame representing the electron density of the metal−metal bond, as shown in part a of Figure 6. If $[FeFe]_H$ adopts an $Fe^{II}Fe^{II}$ valence state without surplus electrons, the metal−metal bond could not be formed, and the Fe−Fe distance ranges between 3.07 and 3.47 Å in some binuclear Fe(II) complexes.[36] However, we found that the Fe−Fe distances in models **2** and **6** of $Fe^{II}Fe^{II}$ remain short (2.55−2.62 Å). As depicted in parts b and c of Figure 5, the HOMOs of the models **2** and **6** involve $Fe(3d)-(H_b)-Fe(3d)$ and $Fe(3d)-2\pi(CO_b)-Fe(3d)$ interactions, respectively. This finding highlights the fact that the hydride and CO_b, which form a 2e−3c bond with two iron ions, are the key to stabilizing the Fe−Fe distance in $[Fe^{II}Fe^{II}]_H$. For $[Fe^{II}Fe^I]-CO_b-H_s$ (**8**[−1,$^1/_2$]), the spin density is mainly located on the two iron ions as shown in Figure 6d (also see Figure 4c). This proves that $[Fe^{II}Fe^{II}]CO_b-H_{ox}$ has a low-lying unoccupied Fe−Fe front orbital and can be seen as an electron sink ($[Fe^{II}Fe^{II}]CO_b-H_{ox} + e \rightarrow [Fe^{II}Fe^I]CO_b-H_s + e \rightarrow [Fe^IFe^I]CO_b-H_{red}$). However, $Fe_p-H_b^--Fe_d$ is stable particularly in $[Fe^{II}Fe^{II}]$. Remarkable differences exist between the electronic configurations of $[Fe^{II}Fe^{II}]H_b^-$ and $[Fe^{II}-Fe^{II}]CO_b-H_{ox}$.

Conclusion

In this paper, we have explored the mechanism of the H−H bond making/breaking in the Fe-only hydrogenase. Model systems incorporating the chemical and biological characteristics of the enzyme are designed and investigated computationally at the DFT level with a basis set of the numeric atomic orbital. Results suggested that both $Fe_p-H_b^--Fe_d$ and $Fe_d-(\eta^2-H_2)$ [also $Fe_p-(\eta^2-H_2)$] species exist in the catalytic cycle and may play important roles for the H_2 activation at the $[FeFe]_H$ active center. The electronic structures of $Fe_p-H_b^--Fe_d$ and $Fe_p-CO_b-Fe_d$ are obviously different. While $Fe_p-H_b^--Fe_d$ is stable in $[Fe^{II}Fe^{II}]$, $Fe_p-CO_b-Fe_d$ can exist in all of the three oxidation states (H_{ox}, H_s, and H_{red}). The ET between $[Fe_4S_4]_H^{2+}$ and $[FeFe]_H$ would be the driving force for the H−H bond making/breaking. The $Fe^{II}Fe^I$ state is active for the dihydrogen reversible oxidation. Regarding the pathways of PT and ET, they are not necessarily the same but must be coupled to lower the overall energy barrier. The sequential routes of H_2 evolution with concerted PT and ET at the diiron active center are eventually presented and discussed.

Acknowledgment. This work is supported by the National Science Foundation of China. We thank the reviewers for their very constructive suggestions to update the paper.

Supporting Information Available: The optimized geometries of the models **1**−**10** in Cartesian coordinates. This material is available free of charge via the Internet at http://pubs.acs.org.

IC0342301